

Postprint: Interference Parameter Variation and Corrosion Behavior of X80 Steel in Guangdong Soil Under HVDC Interference

Authors: Qin Runzhi, Du Yanxia, Lu Minxu, Ou Li, Sun Haiming

Date: 2017-11-21T00:00:00+00:00

Abstract

Indoor simulation experiments were conducted to investigate the variation patterns of interference current density and corrosion behavior of X80 steel in Guangdong soil under large-amplitude high-voltage DC interference voltage. The results indicate that under DC interference potentials of 50–300 V, the current density exhibits a typical three-stage variation characteristic over time: first, it rises sharply within a few seconds to a peak at a relatively high level; then it decreases within a few hundred seconds to a stable value at a relatively low level; and finally it remains around the stable value for a relatively long duration. Combined with measurements and analysis of soil temperature, water content, and resistance near the specimen during the interference process, it is shown that the change in current density is mainly caused by the large-amplitude interference voltage, which leads to a rapid increase in soil temperature around the specimen, a decrease in water content, and a substantial increase in local resistivity within a short period. Simultaneously, the experiments revealed that under DC interference potentials of 50 V, 100 V, 200 V, and 300 V, the corresponding corrosion rates of X80 steel were 5.56, 7.85, 10.63, and 7.78 m/h, respectively; the corrosion rate exhibits a trend of first increasing and then decreasing with the increase of DC interference potential, which differs from the variation pattern of current density peak with DC interference potential but is similar to the variation pattern of current density stable value with DC interference potential. Furthermore, the correlation between the weight-loss corrosion rate of the specimen and the theoretically calculated values of three forms of current density under high-voltage DC interference was analyzed; the results show that the corrosion rate calculated by integrating the current density variation curve during the high-voltage DC interference process has the smallest error compared with the weight-loss corrosion rate; followed by the corrosion rate calculated using the stable value of current density; the corrosion rate calculated using the peak current density has the largest error compared with the

weight-loss corrosion rate, which can reach several times the weight-loss corrosion rate. Based on this, a method for parameter monitoring and corrosion rate prediction under actual high-voltage DC interference is proposed.

Full Text

Study of Interference Parameters Variation Regularity and Corrosion Behavior of X80 Steel in Guangdong Soil under High Voltage Direct Current Interference

QIN Runzhi¹, DU Yanxia¹, LU Minxu¹, OU Li², SUN Haiming²

¹Institute for Advanced Materials and Technology, University of Science and Technology Beijing, Beijing 100083, China

²Sinopec Petroleum Engineering Corporation, Dongying 257026, China

Correspondent: DU Yanxia, associate professor, Tel: (010)62333972, E-mail: duyaxia@ustb.edu.cn

Supported by: National Key Research and Development Program of China (No.2016YFC0802101)

Manuscript received: 2017-07-24, in revised form 2017-10-21

Abstract

High voltage direct current transmission (HVDC) systems have developed rapidly in China in recent years. The ground electrodes of HVDC systems can inject/absorb large amounts of DC current into/from soil, introducing DC interference to nearby pipelines. This can cause remarkable pipe-to-soil potential shifts and high risks of corrosion. In this work, indoor HVDC simulation experiments were carried out based on field tests conducted in recent years. Under high voltages, the variation regularity of DC density and the corrosion behavior of X80 steel in Guangdong soil were studied. The results showed that under 50, 100, 200, and 300 V DC voltages, the DC density of the coupons displayed the same trend and could be divided into three stages. Firstly, the DC density climbed to a peak sharply within several seconds. Then, the DC density decreased gradually to a steady value over hundreds of seconds. Lastly, the DC density remained at that level for the remainder of the test period. Monitoring of the local environment indicated that the variation of DC density was mainly related to local soil temperature increment, water content decrement, and substantial growth of the spread resistance. After interference, the corrosion rates were measured to be 5.56, 7.85, 10.63, and 7.78 m/h, respectively. The corrosion rates increased first and then decreased with interference voltage, following the same pattern as the steady value of DC density but differing from the peak value. Furthermore, three methods for

calculating corrosion rates were studied. The values calculated by integration of the DC density curve had the smallest errors compared with the measured ones. Using steady DC density produced larger errors, and using peak DC density could lead to the biggest errors. Based on these results, a method for predicting HVDC corrosion rates was proposed.

KEY WORDS: HVDC, DC interference, corrosion rate, current density, variation regularity

1. Introduction

High voltage direct current (HVDC) transmission is a high-voltage, high-power, long-distance power transmission technology that utilizes stable direct current. The world's first commercial HVDC transmission project was born in Sweden in 1954, and subsequently, Europe, North America, the former Soviet Union, Japan, Brazil, and other countries and regions have built multiple HVDC projects. HVDC offers significant advantages including large capacity, low losses, simple tower structures, and low line costs, making it particularly suitable for China's large-scale energy projects such as "West-to-East Power Transmission" and "North-to-South Power Transmission." Consequently, HVDC has developed rapidly in China. Since the 1980s, more than a dozen HVDC lines have been established, including TianShengQiao-Guangzhou, Three Gorges-Shanghai, and Hami-Zhengzhou, with additional HVDC projects planned under national strategies such as the "13th Five-Year Plan" and "Belt and Road Initiative" [?].

HVDC systems primarily operate in two modes: bipolar and monopolar. Bipolar operation can be considered as the coupling of two monopolar systems, which automatically switches to monopolar mode during maintenance or faults. When operating in monopolar ground return mode, the earth serves as one conductor, and large DC currents are injected into the ground at one electrode and flow through the earth to the other electrode. These ground currents can be absorbed, transmitted, and released by buried metallic structures, causing severe DC interference and posing risks of personal injury, equipment damage, and metal corrosion.

Foreign cases of HVDC interference with buried pipelines have been reported. For example, when the Trans Mountain crude oil pipeline in North America was interfered with by a nearby 260 kV HVDC transmission project, the pipe-to-soil potential could shift by 400 mV [?]. The Quebec-New England Intertie HVDC system caused DC interference in surrounding areas, with crude oil and natural gas pipelines experiencing pipe-to-soil potential shifts up to 900 mV [?]. An irrigation pipeline in Brazil was interfered with by the Ibiúna grounding electrode 3 km away, with pipe-to-soil potential shifts reaching a maximum of 46 V [?]. When pipe-to-soil potential shifts positively to higher values, the risk of pipeline metal corrosion increases. Hopper et al. [?] conducted simulation

experiments on HVDC interference, demonstrating that leakage current density at pipeline defects was 4-6 orders of magnitude greater than average leakage current density, with smaller defects experiencing greater interference. In their simulation experiments, when the pipe-to-soil potential was 15 V (vs SCE) and the defect area was 0.134 m², the leakage current density reached 23.681 A/m²; when the defect size was 0.0134 m², the leakage current density reached 94.19 A/m², and the pipeline corrosion rate reached 109.25 mm/a.

In recent years, with the successive commissioning of HVDC transmission projects in China, problems of HVDC interference with buried pipelines have continuously emerged. For instance, the Xinjiang section of the West-East Gas Pipeline was interfered with by the Hami-Zhengzhou HVDC project, with pipe-to-soil potential reaching +0.5 V (vs SCE) when the Hami grounding electrode operated in monopolar mode [?]. The Furong-Shanghai section of the West-East Gas Pipeline was interfered with by the Three Gorges-Shanghai HVDC project, causing abnormal output from the cathodic protection system and significant positive potential shifts in the Wuxi-west pipeline, with pipe-to-soil potential reaching a maximum of +830 mV. Guangdong's natural gas pipeline network was interfered with by the Yunnan-Guangzhou HVDC project, resulting in damage to multiple cathodic protection systems and significant potential shifts, with the most positive potential reaching +20 V [?]. A pipeline in Guangdong was interfered with by a nearby HVDC project, with pipe-to-soil potential reaching up to 150 V when the nearby grounding electrode operated in monopolar mode [?]. The Guangdong section of the West-East Gas Pipeline was interfered with by the TianShengQiao-Guangzhou HVDC project, with pipe-to-soil potential reaching up to 304 V (vs SCE), posing a major threat to pipeline operation [?].

China's HVDC projects feature large transmission capacity, high voltage levels, and large ground currents, combined with dense underground pipeline networks, making buried pipelines vulnerable to interference. Compared with foreign HVDC interference cases, Chinese cases clearly exhibit characteristics of high interference parameter amplitudes and large affected areas. Under such high-amplitude HVDC interference, the corrosion risk to buried pipelines remains unclear, and systematic research on the corrosion process under this interference is lacking. Meanwhile, there are currently no effective standards for detection, evaluation, and protection against HVDC interference at home or abroad. With transmission and pipeline projects continuously being commissioned, the situation of pipeline interference by HVDC is becoming increasingly severe, making it urgent to conduct research on the corrosion behavior of pipeline metals under HVDC interference.

This work, based on field-tested HVDC interference parameters, investigated the corrosion behavior of X80 pipeline steel in a Guangdong soil environment under high-amplitude HVDC interference through interference simulation experiments, interference parameter monitoring, and testing of local environmental conditions and corrosion products, aiming to provide reference for understand-

ing and evaluating HVDC interference corrosion risks.

2. Experimental Methods

2.1 Materials and Soil Properties

X80 pipeline steel was selected as the experimental material, obtained from a long-distance pipeline in service. Its main chemical composition (mass fraction, %) was: C 0.070, Mn 1.61, Si 0.21, Ni 0.12, Cu 0.14, Nb 0.041, Ti 0.012, S 0.0025, P 0.0081, Mo 0.13, with Fe as the balance. Coupon dimensions were 18.0 mm diameter \times 3 mm height. Before experiments, samples were ground with SiC waterproof abrasive paper from 360# to 1000#, degreased sequentially with acetone and anhydrous ethanol, rinsed with deionized water, and dried. During experiments, polytetrafluoroethylene fixtures were used to hold the samples, with a metal exposure area of 1 cm².

The experimental soil was reddish-brown clay from Guangdong, collected from a depth of 1 m. The soil had a water content of 21% and resistivity of 24.2 $\Omega \cdot \text{m}$. The soil ion concentrations, converted to inorganic salt content (concentration, mg/L), were: NaCl 0.0114, CaCl 0.0071, MgCl 0.0016, NaHCO 0.0017, Na SO 0.0291, KCl 0.0019, NaNO 0.0286.

2.2 Experimental Setup and Procedures

The experimental apparatus was a self-built HVDC interference soil corrosion simulation system, consisting of a soil test box, interference circuit, and measurement circuit, as shown in [Figure 1: see original paper]. The soil test box (20 cm \times 10 cm \times 8 cm) contained a three-electrode system comprising a working electrode (X80 steel coupon, WE), a saturated calomel reference electrode (RE), and a copper auxiliary electrode (CE), all immersed in the experimental soil. A thermometer was placed 1 cm from the coupon surface to monitor temperature changes during interference. An HSPY 400-01 HVDC interference power supply connected the working and auxiliary electrodes to form the DC interference circuit, which included a 10 Ω shunt resistor and voltmeter in series to evaluate DC current. Combined with the coupon exposure area, this allowed calculation of DC current density. A Reference 3000 electrochemical workstation connected to the three-electrode system formed the measurement circuit, used to test changes in soil spread resistance before and after interference application.

After assembling the experimental apparatus and allowing it to stand for 2 h until the open-circuit potential of the X80 steel coupon stabilized, HVDC interference potentials of 50, 100, 200, and 300 V were applied for 1 h via the HVDC interference power supply. The current in the circuit was obtained by measuring the voltage across the shunt resistor, and the interference current density was calculated based on the coupon area.

To investigate changes in the local soil environment around the coupon during HVDC interference, parameters including soil spread resistance, temperature, and water content were monitored. Soil spread resistance (R_{soil}) represents the resistance between the coupon and reference electrode, related to coupon shape, size, and surface soil resistivity. When external current is high or soil resistivity is high, the measured metal coupon potential includes a significant soil voltage drop (Ohmic potential drop) that cannot be ignored [?, ?]. This can be measured using an applied AC perturbation method [?] as follows:

$$R_{soil} = \frac{U_{AC}}{J_{AC} \cdot A}$$

where U is the applied AC potential of the coupon, J is the AC current flowing through the coupon, and A is the coupon area. During HVDC interference, changes in spread resistance between the coupon and reference electrode were measured using the electrochemical workstation, with a perturbation AC current density of 0.0001 A/cm² (RMS) at 50 Hz frequency.

Simultaneously, a thermometer was used to monitor soil temperature changes at the coupon surface during interference. After interference, soil samples were taken from locations 0.5 cm, 1 cm, and 10 cm from the coupon surface to test soil water content changes.

After interference, corrosion morphologies were observed, and corrosion products on the coupon surface were analyzed using a LabRAM HR Evolution micro-Raman spectrometer with an excitation wavelength of 532 nm and beam diameter of 0.1 μm. To avoid temperature rise on the coupon surface from the laser beam, output power was kept below 1 mW.

Coupons were descaled in an ultrasonic cleaner using a descaling solution (500 mL deionized water + 500 mL concentrated hydrochloric acid + 4-5 g hexamethylenetetramine), cleaned with acetone, rinsed with deionized water, dried, and weighed using an electronic balance with 0.0001 g precision to obtain weight loss. The corrosion rate V during the experimental period was calculated using:

$$V = \frac{W_b - W_a - \Delta W_0}{t \cdot \rho \cdot A}$$

where W_b is the coupon mass before interference, W_a is the mass after interference, ΔW is the weight loss of the blank sample during descaling, t is the experimental period, and ρ is the coupon density.

3. Results and Discussion

3.1 Current Density Variation Under High Interference Voltage

The DC current density of X80 steel coupons in Guangdong soil under 50-300 V DC potential interference is shown in [Figure 2: see original paper]. As seen in the figure, the current density versus time curves followed similar patterns under different interference voltages, all showing high current density in the initial interference stage that decreased significantly after some time. Taking the 300 V interference case in [Figure 2: see original paper]b as an example, the current density curve can be divided into three stages:

Stage 1: Current density rising stage. Within 3 seconds after interference application, the interference current density rapidly rose to a peak value of 868.5 A/m². Stage 1 is characterized by short duration and rapid current density increase.

Stage 2: Current density decreasing stage. After reaching the peak, current density decreased rapidly, reaching a relatively stable value after 480 seconds. Stage 2 is characterized by exponential decrease in current density, with the decreasing rate gradually slowing over time.

Stage 3: Current density stabilization stage. The interference current density remained relatively stable, fluctuating slightly around 36 A/m² until the experiment ended. Stage 3 is characterized by low current density values (only 1/24 of the peak) but long duration.

3.2 Variation of DC Interference Current Density with Interference Voltage

Although the variation patterns of current density under different DC interference voltages were similar, the peak current density in Stage 2 and the steady current density in Stage 3 showed different trends with interference voltage. [Figure 3: see original paper]a shows the variation of peak current density with interference voltage, demonstrating that peak current density increased approximately linearly with interference voltage, reaching a maximum of 868.5 A/m² at 300 V. [Figure 3: see original paper]b shows the variation of steady current density with interference voltage. As interference voltage increased, the steady current density first increased then decreased, reaching a maximum of 68.6 A/m² at 200 V.

3.3 Local Environmental Parameter Variation Around Coupons During HVDC Interference Simulation

Soil temperature at 1 cm from the coupon surface increased to varying degrees during interference, as shown in [Figure 4: see original paper]. At 50 and 100 V interference voltages, soil temperature increased continuously. At 200 and 300 V, soil temperature showed a clear rise-decline pattern. At 200 V, soil temperature reached 34°C within minutes then decreased slightly. At 300 V,

soil temperature first rose rapidly to 52°C, then quickly dropped to 35°C, with slight decreases thereafter. It should be noted that during apparatus setup, to minimize effects on current distribution at the coupon surface, the thermometer was placed 1 cm from the coupon surface, so the measured temperatures were lower than those at the coupon surface and near-surface soil.

After interference, soil samples were taken from within 0.5 cm of the coupon surface and from locations 1 cm and 10 cm away to measure water content, as shown in [Figure 5: see original paper]. The dashed line represents the pre-interference water content, while other curves represent water content at different distances from the coupon. The results show that after HVDC interference application, soil water content decreased significantly at 0.5 cm and 1 cm from the coupon: at the same location, higher DC interference voltage caused greater water content reduction; at the same interference voltage, soil closer to the coupon showed greater water content reduction and more pronounced influence from the coupon. At 10 cm from the coupon, soil water content remained very close to 21%, equivalent to the initial experimental water content. This indicates that under 50-300 V interference, the affected range of soil by coupon reactions was less than 10 cm, with greater effects closer to the coupon surface. For example, at 300 V interference, soil water content decreased from 21% to 12.5% at 1 cm from the coupon surface, and to 9.9% within 0.5 cm of the surface.

The resistance between the coupon and reference electrode (R_c) reflects changes in soil resistivity at the coupon surface. R_c measured before and after interference is shown in [Figure 6: see original paper]. Pre-interference R_c was approximately 3500 Ω , increasing after interference with higher interference voltages producing larger R_c values. Post-interference R_c values were 15398, 22130, 28059, and 83025 Ω at interference voltages of 50, 100, 200, and 300 V, respectively.

3.4 Corrosion Product Analysis and Weight Loss/Corrosion Rate Test Results

After applying 50-300 V HVDC interference for 1 hour in Guangdong soil, X80 steel coupons showed varying degrees of corrosion. The macroscopic morphologies of corrosion products are shown in [Figure 7: see original paper]. The corrosion products were primarily reddish-brown, relatively loose in texture, and not tightly bonded to the steel substrate, allowing easy removal with water. Some corrosion products detached when separating the coupon from surface soil, and some soil components remained on the coupon surface.

Raman spectroscopy analysis of corrosion products is shown in [Figure 8: see original paper]. The peaks were similar under different DC interference potentials, appearing at approximately 215, 285, 390, 605, and 1300 cm^{-1} , with the strongest peak at 285 cm^{-1} . Based on Raman spectroscopy analysis of rust layers in other corrosion processes [?], the main corrosion product under HVDC

interference was $-FeO$.

Weight loss data and corrosion rates obtained after acid cleaning are shown in . The results show that corrosion rate first increased then decreased with interference voltage, reaching a maximum of 10.63 m/h at 200 V and decreasing to 7.78 m/h at 300 V. This pattern was similar to the variation of steady current density values.

4. Discussion

4.1 Mechanism of Current Density Variation

As described above, current density showed a rapid decrease during Stage 2 of HVDC interference, which was closely related to changes in soil physical properties at the coupon surface.

During potential measurement, when external DC current flows through a coupon, the measured DC interference potential (on-potential) includes a soil voltage drop in the medium, as shown in Equation (3) [?, ?]:

$$E_{on} = E_p + I_{DC} \cdot R_{soil}$$

where E_{on} is the measured DC interference potential (on-potential), E_p is the polarization potential, I_{DC} is the DC current flowing through the coupon, $I_{DC} \cdot R_{soil}$ is the voltage drop in soil representing the potential division between the working electrode surface and reference electrode, and J_{DC} is the DC current density.

During 50-300 V HVDC interference, the DC interference voltage (E_{on}) remained essentially constant, while E_p measured by the interruption method was approximately -0.5 to 0.5 V (vs SCE), much smaller than E_{on} . Therefore, J_{DC} can be expressed as:

$$J_{DC} \approx \frac{E_{on}}{R_{soil} \cdot A}$$

In HVDC interference, J_{DC} is inversely proportional to R_{soil} . As shown in [Figure 6: see original paper], R_{soil} increased substantially after interference (by several tens of times), consistent with the large decrease rate of J_{DC} .

Calculated steady-state J_{DC} values using Equation (4) are shown in . The calculated J_{DC} values were very close to measured values with small errors, showing the same trend of first increasing then decreasing with interference potential. This confirms the correlation between current density and soil physical properties—that the substantial decrease in DC current density during interference was caused by the significant increase in R_{soil} .

Nielsen et al. [?] proposed that when external current flows through a coupon in soil, R_{sfc} reflects the properties of soil at the coupon surface and is closely related to soil resistivity, temperature, ion concentration, and other parameters. Cao et al. [?] noted that when DC current passes through soil, it affects ion concentration and transport numbers, thereby causing changes in soil resistivity. Huang et al. [?] suggested that soil resistivity first increases then decreases with increasing DC current density, but did not consider the thermal effect of DC current. Sima et al. [?, ?] pointed out that when DC current density is high, thermal effects occur in soil, accelerating water evaporation and causing substantial increases in soil resistivity. Combined with [Figure 4: see original paper] and [Figure 5: see original paper], the results show that during interference, soil temperature at the coupon surface increased, water content decreased significantly, and soil resistivity at the coupon surface increased substantially, causing R_{sfc} to increase markedly.

Based on the above analysis, the reasons for current density variation can be summarized as: (1) **Stage 1:** When interference is first applied, high external DC potential causes rapid electrochemical reactions at the coupon/soil interface, quickly raising current density to a peak; (2) **Stage 2:** The high peak current density generates significant heat from electrochemical reactions and resistance heating, increasing temperature at the coupon and soil surface, accelerating water evaporation in soil, reducing water content, and increasing soil resistance. With constant interference voltage, current density gradually decreases; (3) **Stage 3:** When current density decreases to a stable value, heat generation at the coupon surface decreases and reaches equilibrium with outward heat conduction. Since water forms a concentration gradient in soil around the coupon, osmosis occurs, and equilibrium is established between osmotic and evaporation effects, allowing current density to remain relatively stable.

In HVDC interference, pre-interference R_{sfc} values were roughly equal, so peak current density was primarily related to interference potential, increasing with higher interference potential. However, steady-state current density resulted from the combined effects and balanced equilibrium of interference potential, heat generation and diffusion, water osmosis, and soil structure/physicochemical properties. Therefore, steady-state current density did not show a positive correlation with interference potential, reaching its highest value at medium DC interference potential (200 V) under these experimental conditions.

4.2 HVDC Interference Corrosion Risk and Correlation Between Corrosion Rate and Current Density

The magnitude of HVDC interference corrosion risk and establishment of effective assessment methods are primary concerns in practical applications. According to the experimental results in [?], in Guangdong soil, corrosion rates were 5.56, 7.85, 10.63, and 7.78 m/h at interference potentials of 50, 100, 200, and 300 V, respectively. Generally, HVDC transmission engineering design standards specify 1% monopolar operation time per year [?]. Based on this, the estimated

annual corrosion rates for coupons at interference potentials of 50, 100, 200, and 300 V are approximately 0.486, 0.687, 0.931, and 0.681 mm/a, respectively.

The results also show that corrosion rate during HVDC interference first increased then decreased with increasing DC interference potential, reaching a maximum at 200 V and decreasing at 300 V. This pattern differed significantly from the linear relationship between peak current density and interference potential shown in [Figure 3: see original paper]a, but was very similar to the variation pattern of steady-state current density with interference potential shown in [Figure 3: see original paper]b.

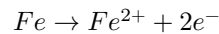
Since current density is an important parameter affecting corrosion rate, three theoretical corrosion rates were calculated based on Faraday's law using: (1) the current density variation curve, (2) peak current density, and (3) steady-state current density from [Figure 2: see original paper].

According to Faraday's law, the electrochemical reaction rate R is:

$$R = \frac{i}{nF} = \frac{j \cdot A}{nF}$$

where i is the current flowing through the coupon, j is current density, n is the number of electrons consumed or generated in the electrochemical reaction, and F is the Faraday constant.

Considering the possible reactions:



The theoretical corrosion weight loss w of X80 steel under different interferences is:

$$w = \int_0^t \frac{j \cdot A \cdot M}{nF} dt$$

where M is the molar mass of the reactant and t is the reaction time. Theoretical corrosion rates were calculated using Equations (7) and (2). Taking the 300 V DC interference case as an example, for the three current density scenarios, the current density curve method used integration of the current density curve, as shown in [Figure 9: see original paper]. Peak current density used 868.5 A/m², and steady-state current density used 36 A/m².

Corrosion rates calculated from the three current density methods and their relative errors compared with weight loss corrosion rates are shown in . The corrosion rate calculated by integrating the current density variation curve was closest to the weight loss method, with the smallest error. The corrosion rate calculated using steady-state current density had some deviation, with errors of

14.57%-38.70%. The corrosion rate calculated using peak current density had large errors, reaching several times the actual corrosion rate.

These results demonstrate that in actual HVDC interference, corrosion rates can be predicted by monitoring current density combined with Faraday's law. The most accurate method is to monitor the current density variation curve over time and calculate corrosion rate through area integration. If the steady-state current density in the middle-to-late interference stage can be detected, it can also be used to roughly estimate corrosion rate, which still has some engineering application value despite certain errors. However, using the peak current density from the initial interference stage to evaluate corrosion rate is not recommended, as it would cause significant overestimation.

5. Conclusions

1. Under 50-300 V DC interference potential in Guangdong soil, X80 steel coupons exhibited typical three-stage current density variation over time: rapid rise to a high peak within several seconds, followed by decrease to a lower steady value over hundreds of seconds, and finally maintenance at that steady value for an extended period. Analysis of soil temperature, water content, and resistance near coupons during interference indicated that current density variation was primarily caused by substantial interference voltage inducing rapid temperature increase around the coupon, water content reduction, and substantial local resistivity increase.
 2. Under the experimental conditions, corrosion rates were 5.56, 7.85, 10.63, and 7.78 m/h at DC interference potentials of 50, 100, 200, and 300 V, respectively. Corrosion rate first increased then decreased with increasing DC interference potential, a trend different from the variation pattern of peak current density but similar to that of steady-state current density.
 3. Based on Faraday's law, theoretical corrosion rates corresponding to three forms of current density were calculated and compared with weight loss corrosion rates. The results showed that corrosion rates calculated by integrating the current density variation curve during HVDC interference had the smallest error compared with weight loss rates. Corrosion rates calculated using steady-state current density had larger errors, while those using peak current density had the largest errors, reaching several times the weight loss corrosion rate. Accordingly, a method for parameter monitoring and corrosion rate prediction under actual HVDC interference was proposed.
-

References

- [1] Zhao W J. High Voltage Direct Current Engineering Technology [M]. Beijing: China Electric Power Press, 2004: 1
- [2] Shu Y B, Liu Z H, Gao L Y, et al. A preliminary exploration for design of ± 800 kV UHVDC project with transmission capacity of 6400 MW [J]. Power Sys. Technol., 2006, 30(1): 1
- [3] Liu Z H, Gao L Y, Yu J. Study on ± 800 kV UHVDC transmission technology [J]. Electric Power Construction, 2007, 28(10): 17
- [4] Zhan Y, Yin X G. Comparative research on HVDC and UHVC power transmission [J]. High Voltage Eng., 2001, 27(4): 44
- [5] Larruskain D M, Abarrategui O, Zamora I, et al. Transmission and distribution networks: AC versus DC [A]. 9th Spanish Portuguese Congress on Electrical Engineering [C]. Marbella: AEDIE and APDEE, 2005: 245
- [6] Zhou H, Zhong Y J. Applicable occasions of UHVAC/UHVDC transmission and their technology comparisons in China [J]. Electric Power Automation Equip., 2007, 27(5): 6
- [7] Verhiel A J. The effects of high-voltage DC power transmission systems on buried metallic pipelines [J]. IEEE Trans. Ind. General Appl., 1971, (3): 403
- [8] Nicholson P. High voltage direct current interference with underground/underwater pipelines [A]. Proceedings of the Corrosion 2010 [C]. San Antonio: NACE International, 2010: 10102
- [9] Caroli C E, Santos N, Kovarsky D, et al. Itaipu HVDC ground electrodes: Interference considerations and potential curve measurements during Bipole II commissioning [J]. IEEE Trans. Power Delivery 1990, 5:1583
- [10] Hopper A T, Gideon D N, Berry W E, et al. Analysis of the effects of high-voltage direct-current transmission systems on buried pipelines [R]. Falls Church: PRCI, 1967
- [11] Bi W X, Chen H Y, Li Z J, et al. HVDC interference to buried pipeline: numerical modeling and continuous p/s potential monitoring [A]. Proceedings of the Corrosion 2016 [C]. Vancouver: NACE International, 2016: 7714
- [12] Ying B. The influence of HVDC system ground electrode on safe operation of long-distance pipeline [J]. Oil-Gas Field Surf. Eng., 2014, 33(7): 23
- [13] Gong Y, Xue C, Yuan Z, et al. Advanced analysis of HVDC electrodes interference on neighboring pipelines [J]. J. Power Eng, 2015, 3(4):332
- [14] Qin R Z, Du Y X, Peng G Z, et al. High voltage direct current interference on buried pipelines: Case study and mitigation design [A]. Proceedings of the Corrosion 2017 [C]. New Orleans: NACE International, 2017: 9049

- [15] Bard A J, Faulkner L R. Electrochemical methods: fundamentals and applications [M]. New York: Wiley, 2000: 16
- [16] Cao C N. Principles of electrochemistry of corrosion [M]. 3rd Ed., Beijing: Chemical Industry Press, 2008: 158
- [17] Nielsen L V, Rosenberg H, Baumgarten B, et al. AC Induced Corrosion in Pipelines: Detection, Characterization and Mitigation[A]. Proceedings of the Corrosion 2004 [C]. New Orleans: NACE International, 2004: No.04211
- [18] Nielsen, L V, Galsgaard F. Sensor technology for on-line monitoring of AC induced corrosion along pipelines [A]. Proceedings of the Corrosion 2005 [C]. Houston: NACE International, 2005: No.05375
- [19] Nielsen, L V, Nielsen, K V. Differential ER-technology for measuring degree of accumulated corrosion as well as instant corrosion rate [A]. Proceedings of the Corrosion 2003 [C]. San Diego: NACE International, 2003: No.03443
- [20] Nielsen, L. V. Role of alkalization in AC induced corrosion of pipelines and consequences hereof in relation to CP requirements [A]. Proceedings of the Corrosion 2005 [C]. Houston: NACE International, 2005: No.05188
- [21] Froment F, Tournié A, Colomban P. Raman identification of natural red to yellow pigments: ochre and iron-containing ores [J]. J. Raman Spectrosc, 2008, 39: 560
- [22] Duennwald J, Otto A. An investigation of phase transitions in rust layers using Raman spectroscopy [J]. Cheminform, 1989, 29:1167
- [23] Xing X C, Li X G, Xiao K, et al. Corrosion behaviors at the initial stage of q235 steel in Xisha atmosphere [J]. J. Chin. Soc. Corros Prote, 2009, 29: 465
- [24] Chitra P, Rajaram R, Venkatesh P. Raman identification of corrosion products on automotive galvanized steel sheets [J]. J. Raman Spectrosc, 2010, 39: 881
- [25] Cao X B, Wu G N, Fu L H, et al. The impact of dc current density on soil resistivity [J]. Proceeding CSEE, 2008, 28(6): 37
- [26] Huang Z, Wu G, Jiang W, et al. Study of the influences on soil resistivity caused by HVDC mono-polar operation [A]. International Conference on High Voltage Engineering and Application [C]. Chongqing: IEEE, 2009: 232
- [27] Sima W, Luo L, Yuan T, et al. Experimental analysis on the change regulation of the soil resistivity considering the thermal effect around the grounding electrode [A] Asia-Pacific International Conference on Lightning [C]. Chengdu: IEEE, 2011: 673
- [28] Sima W X, Luo L, Yuan T, et al. Temperature characteristic of soil resistivity and its effect on the DC grounding electrode heating [J]. High Voltage Eng., 2012, 38: 1192

[29] NACE SP0169-2013, Control of external corrosion on underground or submerged metallic piping systems [S]. Houston: NACE International, 2013

Note: Figure translations are in progress. See original paper for figures.

Source: ChinaXiv – Machine translation. Verify with original.